If He is lost primarily by thermal escape, we estimate that the atmospheric residence time should be of the order of 10^5 seconds. The source strength required to supply the observed He atmosphere would then be of the order of 10^7 cm^{-2} sec^{-1}, which is comparable to the He source in the earth's atmosphere (*6*).

The drift sequence across the bright limb (Fig. 2b) provides stringent upper limits to the abundances of probable atmospheric constituents. These are listed in Table 1 and were estimated from data taken 15 km above the limb. For these calculations we have assumed the local surface temperature at the limb to be 550°K (*7*). Scattering efficiencies and *g*-values for the resonance emissions of H, O, C, and Xe were scaled from the compilations of Barth (*8*) and Fastie *et al.* (*9*). For the other species the *g*-values were based on reported solar fluxes (*10*), oscillator strengths (*11*), and assumed solar line widths (*12*).

Inspection of the results in Table 1 shows that the airglow spectrometer is far more sensitive to individual species than the occultation instrument. Of particular interest is Ar, which should be produced radiogenically in the planet. If we assume that Ar is removed primarily by interaction with the solar wind, we can deduce an upper limit to the supply rate. Its residence time should be similar to the ionization time of the gas, that is, $\sim 10^6$ seconds. Combining this number with the column density upper limit in Table 1, we find a maximum source strength of $\sim 10^7$ cm^{-2} sec^{-1}. This is consistent with the terrestrial supply rate of 2×10^5 cm^{-2} sec^{-1} (*6*).

During the Mercury encounter channels at wavelengths short of 1216 Å observed sporadic emission. This emission was seen during the limb drifts and while observations were being made of the dark side of the planet. The spacecraft was also within the solar wind cavity during most of these bursts of emission, but we have found little correlation with the fluxes observed by the plasma and energetic particle experiments (*13*).

Extreme ultraviolet albedo. Observations of the bright side of the moon were obtained with the airglow instrument shortly after launch. These were compared with similar measurements on Mercury made several hours before encounter. The ratio of the apparent brightnesses is plotted in Fig. 4 on an arbitrary scale. The marked similarity between the two is obvious in spite of the poor statistics in the two short-wavelength channels at 304 and 430 Å. Evidently the similarity of the run of albedo with wavelength between Mercury and the moon that has been reported throughout the visible (*14*) extends far into the ultraviolet and probably at least down to wavelengths of 500 Å.

Conclusions. The Mariner 10 ultraviolet spectrometer experiment has achieved its primary objective of detecting a neutral atmosphere on Mercury. Evidently neutral He is a prime constituent. The column density is very low, such that the atmospheric atoms follow ballistic trajectories. The occultation experiment places an exceedingly low limit to the total atmospheric content, far lower than indicated by any previous measurements. Further reductions in these limits are expected when the effects of spacecraft limit cycle motion are included in the analysis. Similarly, further analysis should provide information on the neutral He scale height and also on the origin of the unexpected "emission" seen as the spacecraft flew behind Mercury.

A. L. BROADFOOT
S. KUMAR
M. J. S. BELTON
Kitt Peak National Observatory, Tucson, Arizona 85726
M. B. MCELROY
Harvard University, Cambridge, Massachusetts 02138

References and Notes

1. A. L. Broadfoot, S. Kumar, M. J. S. Belton, M. B. McElroy, *Science* **183**, 1315 (1974).
2. J. A. R. Samson, *Techniques of Vacuum Ultraviolet Spectroscopy* (Wiley, New York, 1967), p. 76.
3. The solar disk had an angular diameter of 1.18° at Mercury encounter. The intensity distribution in the extreme ultraviolet is very inhomogeneous over the disk [see E. M. Reeves and W. H. Parkinson, *Astrophys. J. Suppl.* **21**, 1 (1970)]. The spacecraft limit cycle was ± 0.3° in all three axes.
4. U. Fink, H. P. Larsen, R. F. Poppen, *Astrophys. J.* **187**, 407 (1974).
5. M. J. S. Belton, D. M. Hunten, M. B. McElroy, *ibid.* **150**, 1111 (1967).
6. P. M. Banks, H. E. Johnson, W. I. Axford, *Comments Astrophys. Space Phys.* **2**, 214 (1970).
7. S. C. Chase, E. D. Miner, D. Morrison, G. Münch, G. Neugebauer, M. Schroder, *Science* **185**, 142 (1974).
8. C. A. Barth, *Appl. Opt.* **8**, 1295 (1969).
9. W. G. Fastie, P. D. Feldman, R. C. Henry, H. W. Moos, C. A. Barth, G. E. Thomas, T. M. Donahue, *Science* **182**, 710 (1973).
10. H. E. Hinteregger, *Ann. Geophys.* **26**, 547 (1970).
11. W. L. Wiese, M. W. Smith, B. M. Glennon, *Ref. Data Ser. U.S. Natl. Bur. Stand.* **1**, 4 (1966).
12. For the He 584-Å line, we have used the solar line width measured by G. Cushman, L. Farwell, G. Goden, and W. A. Rense (in preparation).
13. We wish to thank J. A. Simpson and H. S. Bridge for providing us with their unpublished data.
14. T. B. McCord and J. B. Adams, *Science* **178**, 745 (1972); *Icarus* **17**, 585 (1972).
15. We would like to express our appreciation for the assistance of Frank E. Stuart and the Electronics Laboratory at Kitt Peak National Observatory in construction of the instrument. We are especially grateful for the exceptional effort put forth by Sam S. Clapp, senior engineer at Kitt Peak. Special thanks are due to Jet Propulsion Laboratory personnel, particularly Clayne M. Yeates and James A. Dunne for providing the science support. We also thank D. G. Rea for a critical review of the manuscript. This research was sponsored by the National Aeronautics and Space Administration. Kitt Peak National Observatory is operated by the Association of Universities for Research in Astronomy, Inc., under contract with the National Science Foundation.

3 June 1974

Mercury's Surface: Preliminary Description and Interpretation from Mariner 10 Pictures

Abstract. *The surface morphology and optical properties of Mercury resemble those of the moon in remarkable detail and record a very similar sequence of events. Chemical and mineralogical similarity of the outer layers of Mercury and the moon is implied; Mercury is probably a differentiated planet with a large iron-rich core. Differentiation is inferred to have occurred very early. No evidence of atmospheric modification of landforms has been found. Large-scale scarps and ridges unlike lunar or martian features may reflect a unique period of planetary compression near the end of heavy bombardment by small planetesimals.*

Mariner 10 acquired 2300 television pictures in the vicinity of Mercury in order to investigate the geologic history of the planet as manifested in the morphology and optical properties of the surface. A unique surface history could have been indicated by the planet's Earth-like density (5.5 g/cm^3) and small size (4870 km) (*1*). Instead, an extraordinary similarity to the surface of the moon has been found; the implications of this lunar-like exterior and probable Earth-like interior provide insight into very early stages of planetary formation.

A brief description of the first images

Table 1. Sequence summary.

Phase	Range (km)	Resolution (km)	Frames
Incoming far encounter, −6 days to −1 day	4,500,000–800,000	127–20	716
Incoming color mosaicking, −1 day to −3 hours	800,000–100,000	20–4	212
Close encounter, −3 hours to +3 hours	100,000–10,000	4–0.15	548
Outgoing color mosaicking, +3 hours to +1 day	100,000–800,000	4–20	220
Outgoing far encounter, +1 day to +3 days	800,000–2,000,000	20–60	112
Satellite search, +1 day to +3 days	1,000,000–3,500,000		555
Total			2363

Table 2. Normal albedos.

Feature (Fig. 5)	Earth-based	Mariner 10
Lunar		
Mare Crisium	0.085	0.10
Mare Serenitatis	0.09	0.10
Highlands between Crisium and Serenitatis	0.16	0.17
Brightest crater	0.23	
Integrated disk*	0.125	
Mercurian		
Bright craters and rays (1, 6, 7, 11, 14, 22, 23, 28, 29, 30, 31)		0.19–0.25
Heavily cratered terrain and textured plains (4, 9, 10, 12, 13)		0.11–0.19
Flat-floored craters (3, 2)		0.10, 0.13
Smooth plains (15, 16, 17, 18, 20, 26, 27, 33)		0.08–0.12
Integrated disk*	0.125	

* From (5).

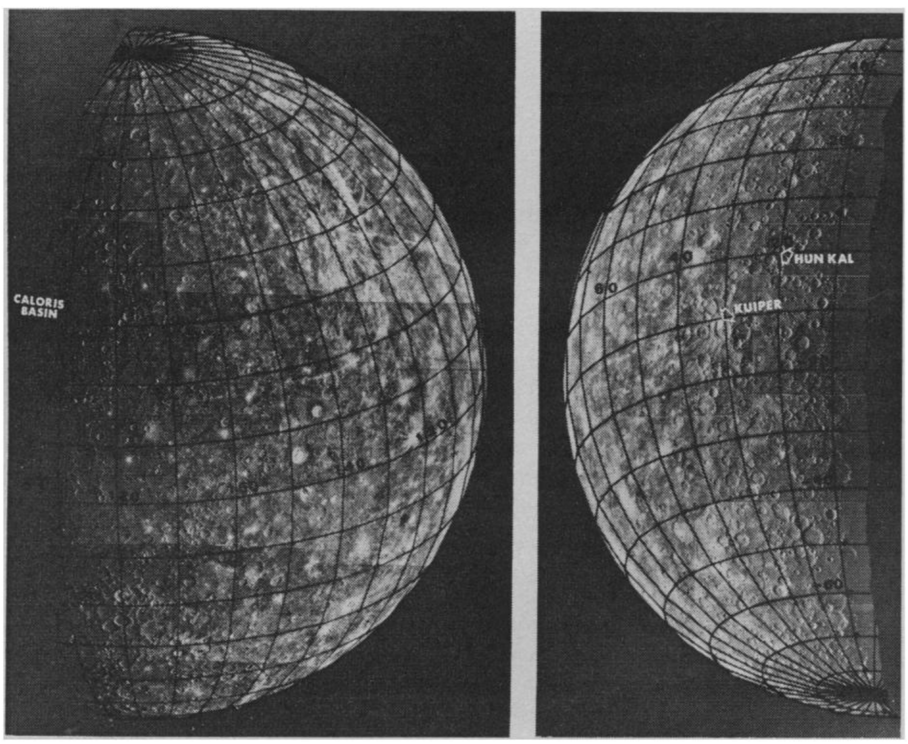

Fig. 1. Photomosaic of the incoming (right) and outgoing (left) view of Mercury with the approximate coordinate system. The provisionally named features discussed in the text are indicated.

has already been published (*2*). We present here further experimental results and consequent interpretations from preliminary study of all the pictures received in the March 1974 encounter as well as a quantitative analysis of about one-tenth of the total. Table 1 summarizes the data set. High-resolution photomosaics covering nearly all the lighted hemisphere of the planet were constructed from specially processed frames of the close encounter phase (Figs. 1 and 2). In regions of favorable lighting and viewing geometry the resolution is 1.5 to 2.0 km, comparable to good Earth-based photography of the moon. There are about 200 additional individual pictures of resolution ranging from 1.5 to 0.15 km.

Pictures from the satellite search phase of the imaging experiment reveal no mercurian satellites, only stars (Fig. 3). We place an upper limit of 5 km on the diameter of any hypothetical mercurian satellite with an albedo similar to that of the planet. Spatial coverage is estimated to be at least 95 percent complete for equatorial satellites within 30 planetary radii. Further processing is expected to improve the detection limit to about 2 km in diameter and to increase the completeness of spatial coverage.

The photographic coverage provided by Mariner 10 is so extensive that a mercurian surface coordinate system and control net is necessary. Coordinates of features (control points) on Mercury are being computed photogrammetrically by methods similar to those developed for use with Mars (*3*). As of May 1974, 635 measurements of 151 points on 45 pictures had been incorporated into the control system. A series of maps, to be produced by the U.S. Geological Survey, is planned as the cartographic base for future systematic geologic mapping.

In the Mariner 10 coordinate system the axis is assumed always to be normal to the orbital plane of Mercury (0° obliquity). The crater Hun Kal, about 1½ km in diameter, has been chosen to define the system of longitudes; the 20° meridian passes through its center at latitude about 0.4°S (Fig. 4). Thus, the 20° meridian defines the longitude on Mercury in the same way that the 0° meridian (Greenwich) does on Earth (*4*).

Surface optical properties. Earth-based observations indicate that the integral optical properties of Mercury are closely similar to the global average of the moon (*5–7*). The average microrelief and surface composition of the two objects, therefore, have been inferred to be similar. Mariner 10 provided an opportunity to determine whether this similarity extends to regional variations in optical properties such as the highland/maria dichotomy of the moon. In addition to a comprehensive preflight photometric and geometric calibration, extensive photography of Earth and the moon was carried out from Mariner 10 shortly after launch to permit direct comparison between Mercury and the moon.

The relative brightness distribution in a selected image of Mercury, taken on the incoming leg of the trajectory, is virtually identical with similar plots of lunar data made from both Mariner 10 and Earth-based observations at similar phase angle. Moreover, the ultraviolet (UV) plane polarization of Mercury in the phase angle range from 80° to 100° is indistinguishable from that of the moon down to a scale of at least 50 km. Evidently the mercurian surface observed by Mariner 10 is everywhere covered with a fine-grained material analogous to the lunar regolith.

The normal albedos (*8*), corrected to a wavelength of 0.55 μm, were measured for 33 representative areas. Their locations are shown in Fig. 5, and the results of the measurements are summarized in Table 2. Relative accuracy is estimated to be 10 to 15 percent; absolute errors may be somewhat larger. Crater Kuiper (number 1, Fig. 5) is one of the brightest areas on the visible hemisphere of Mercury with a normal albedo of 0.24. Both the interior of Caloris Basin and of the smooth plains outside the basin rim have albedos of 0.12. Heavily cratered terrain has approximately the same average albedo as the lunar highlands, and the smooth plains of Mercury are significantly darker. However, Mercury's appearance is blander than that of the moon. Albedo boundaries between light and dark regions are less distinct on Mercury than on the moon, as illustrated in Fig. 6.

We investigated regional color variations by forming ratios of pictures taken with the orange (OR) filter to those taken with the UV filter (see Fig. 7 for the spectral responses of each filter). No pronounced regional color differences were apparent, the maximum dispersion in the OR/UV ratio being approximately ± 5 percent. In particular, no areas with nearly flat

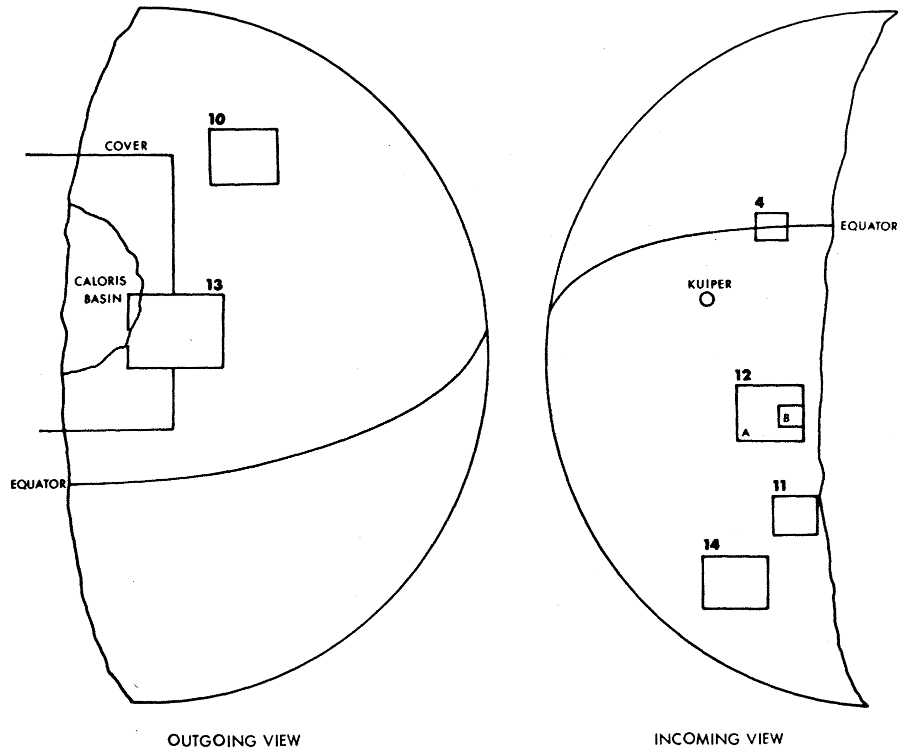

Fig. 2. Index map showing the location and figure numbers (in boldface) of the photographs discussed in the text.

reflection spectra and high plane polarization, which might indicate the presence of significant amounts of metallic iron on the surface, were noted. As for the moon, brighter areas on Mercury are generally redder than average, although many exceptions to this rule occur. For example, Crater Kuiper (latitude, −11°; longitude, 31°) is redder, but the bright crater near latitude 36°, longitude 127° is bluer. The basin 440 km in diameter at latitude −15°, longitude 165° has a light, reddish interior surrounded by a darker, bluish border (Fig. 8). The interior plains of Caloris Basin are also redder than average. Such faint color differences probably correspond to compositional differences in the surface materials on Mercury similar to those

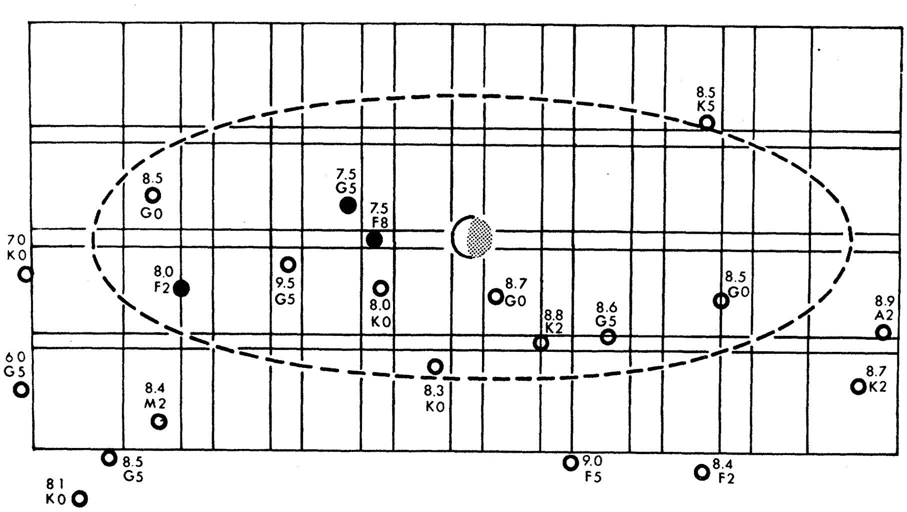

Fig. 3. A 36-picture satellite search sequence, taken 3.5×10^6 km from Mercury, is diagramed with background stars. The actual pointing for individual pictures is still slightly uncertain because of slight spacecraft angular motion. A satellite in a circular orbit at 30 Mercury radii would lie on the ellipse. The closed circles are three stars detected in preliminary processing of the television pictures, and the open circles are undetected stars. The visual magnitude and spectral type of the star are indicated adjacent to each circle. The detectability of the stars sets an upper limit of about 5 km in diameter for a hypothetical satellite.

Table 3. Crater units.

Surface location (Fig. 5)	Number of craters counted	Area (km^2)
Heavily cratered (area A)	1538	4.28×10^6
Plains (area B)	107	2.33×10^4
Plains (area C)	56	1.14×10^4
Caloris Basin	95	4.04×10^5
Area D	261	1.23×10^5
Plains east of Caloris Basin	416	8.50×10^5
Area E	2432	3.11×10^4
Plains (area F)	429	6.33×10^3

found on the moon within individual maria or associated with fresh craters. Thus, Mercury exhibits a surprising similarity to the moon in regional color variations as well as albedo variations. Mercury does indeed resemble the moon on a regional as well as on a global basis. Regional differences in optical properties on the moon generally reflect chemical and mineralogical variations within the overall iron silicate composition of surface material. Grossly similar variations are suggested for the surface of Mercury by the Mariner 10 picture data.

Craters and circular basins. Craters are the predominant landform on Mercury. The areal density differs from one part of the surface to another (Fig. 9), in much the same way as for the highlands and maria on the moon. With increasing size, craters grade into basins—circular structures with an arbitrary lower limit which, for the purposes of this report, is 200 km in diameter. The craters on Mercury are morphologically similar to lunar craters of the same size and evidence the same stages of degradation as their lunar counterparts. This indicates that similar formation and erosive processes have been active, especially meteoroid impact.

Craters smaller than ~10 km in diameter grade from shallow, barely discernible depressions to bowl-shaped cavities exhibiting well-developed raised rims, ejecta deposits, secondary crater fields, and, around some craters, ray systems contrasting in albedo with the surrounding surface. Larger degraded craters, which have lost their ejecta deposits and seondary crater fields and have no prominent raised rims, are typically shallow, flat-floored, and sometimes filled with plains materials. Fresher and presumably younger features commonly exhibit essentially flat floors and terracing on the interior walls; central peaks or ringed complexes are prevalent. The continuous ejecta deposits of the larger craters do not extend as far from the crater rim as for otherwise similar lunar craters. Similarly, the radial distance to the position of maximum areal density of secondary craters is closer to the rim of mercurian craters, and preliminary depth-diameter measurements for 131 craters ranging from 3 to 200 km suggest that mercurian craters are significantly shallower than similar-sized lunar craters. All three differences are consistent with Mercury's greater gravitational acceleration, which can reduce the ballistic range of ejecta and also cause a greater degree of post-cratering collapse through slumping of the rim of the impact cavity.

We obtained crater size-frequency distributions, using the techniques and procedures described by Greeley and Gault (*9*), as a basis for determining the relative ages of major physiographic provinces and several selected surface units (Table 3 and Fig. 9). Areas in which the crater counts were made are indicated in Fig. 5. The heavily cratered terrain observed prior to encounter is not only grossly similar in general appearance to the lunar highlands but also has a crater frequency distribution (Fig. 9) essentially identical to that of the southern highlands on the nearside of the moon. Both surfaces have attained equilibrium or steady-state conditions (*10, 11*), with craters as large as at least 100 km in diameter; landforms there have survived since the end of intense bombardment by small planetesimals.

Table 4 lists all basins larger than 200 km in diameter within the areas of favorable viewing areas outlined in Fig. 8. The basins show a variety of morphologies depending on their size, relative age, and degree of flooding by plains materials. The smaller basins tend to have two well-preserved rings, with the diameter of the outer ring close to twice that of the inner ring (Fig. 10). Both rings are of relatively low relief. Radar measurements give a height of 1.5 km relative to the basin floor for the outer ring of basin 5 of Fig. 8 (*12*). In some basins, the inner ring is partially covered with plains materials and the area between the two rings contains irregular hills. Outside the outer ring, radial structures dominate, consisting of hills, valleys, gouges, and strings of craters. Secondary craters and gouges occurs as close as one-fourth crater diameter to the outer ring and extend outward in a continuous field to one crater diameter in the freshest examples (Fig. 10).

Caloris Basin, the largest structural feature apparent in the Mariner 10 pictures, is similar in appearance and size to the lunar Imbrium Basin and undoubtedly originated by impact of a body at least tens of kilometers in diameter. The basin is bounded by a ring of mountains about 1300 km in diameter which forms an irregular scarp averaging around 2 km in height above the basin floor (see cover). Between about 23° and 30°N, the scarp is very subdued and appears to be mantled by plains material. In the northeastern part of the basin, a weak outer scarp occurs at a distance of about 150 km beyond the main scarp. Between these two scarps is a terrain characterized by relatively smooth hills or domes similar in appearance to the terrain adjacent to the Rook Mountains in the lunar Orientale Basin. Surrounding the main scarp and extending outward for at least one basin diameter is

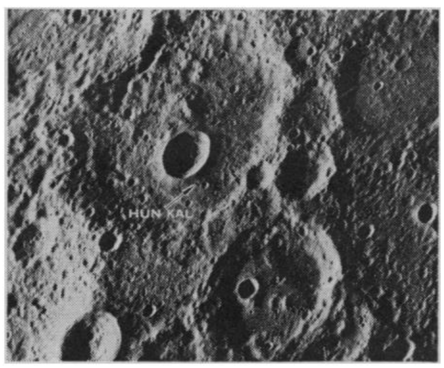

Fig. 4. The 20° meridian passes through the center of the small 1.5-km crater Hun Kal in the Mariner 10 coordinate system. Hun Kal means the numeral 20 in the language of the Maya Indians of Central America; the ancient Maya used a base 20 number system. Hun Kal lies less than 1° south of the equator and defines the Mariner 10 topocentric system of longitudes on Mercury. Numerous elongate craters of probable secondary impact origin are typical of many areas on the planet.

a radial system of linear hills which is best developed northeast of the basin. The radial system is only weakly developed in the terrain between the two scarps; its main development begins beyond the outer scarp in this area. This radial system of hills is embayed by smooth plains material which completely surrounds at least the visible eastern portion of the basin.

Stuart-Alexander and Howard (*13*) counted 24 well-defined basins 300 km in diameter and larger on the moon. In contrast, we have observed eight basins larger than 300 km over approximately one-third of the surface of Mercury, suggesting about the same total of 24 for a body with a surface area twice that of the moon. However, we observe no basins in the size range 500 to 1300 km; the total for the moon in this size range is five (*13*). The relative deficiency of large basins on the surface of Mercury so far viewed probably has affected the regional appearance of the planet as compared to that of the moon. Ejecta blankets and secondary craters are observable around virtually all basins that are not flooded by plains materials outside the outer ring. Obliteration of these features by subsequent basins larger than 500 km apparently has not occurred on the observed surface of Mercury to the same degree as on the moon (*14*).

Plains. The floors of many basins and craters and the surfaces around several large basins are relatively level, except for scarps and ridges. These surfaces tend to be free of craters larger than 10 km in diameter and are referred to as plains; they are obviously younger than the surrounding heavily cratered terrain. The mercurian plains seen in Mariner 10 pictures strongly resemble the lunar maria. It is important to determine whether a similar volcanic origin also can be inferred for at least some of the mercurian plains. In the following we review morphological evidence which bears on the origin of the plains.

The general distribution of plains visible in the Mariner 10 pictures is plotted in Fig. 8. Many craters in the diameter range 100 to 200 km are filled with plains materials, but others are not, including some that appear to be as old as those that are filled. The plains materials on Mercury fill all of the basins on the planet but to different degrees (see, for example, Fig. 13). Particularly important is the difference between the 350-km north polar basin (number 3, Table 4), which is filled and surrounded by a broad belt of plains, and a basin of identical size at 45°S (number 14, Table 4), which contains only a restricted area of plains on its floor. These relations are more easily explained if the plains are presumed to have formed in episodes of volcanism that followed formation of most of the basins rather than as impact melts at the time of each major cratering event.

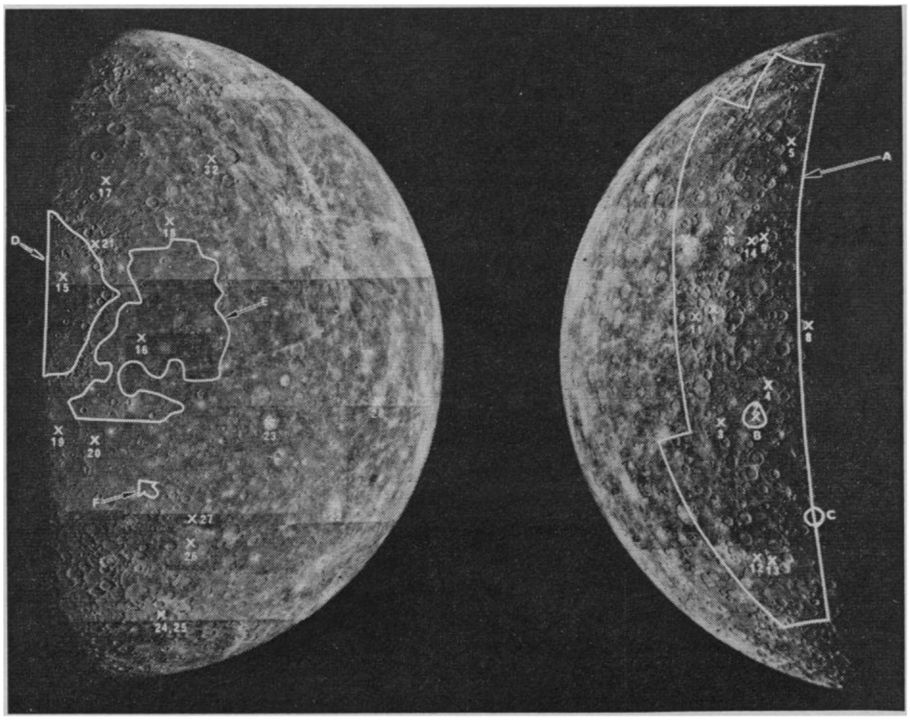

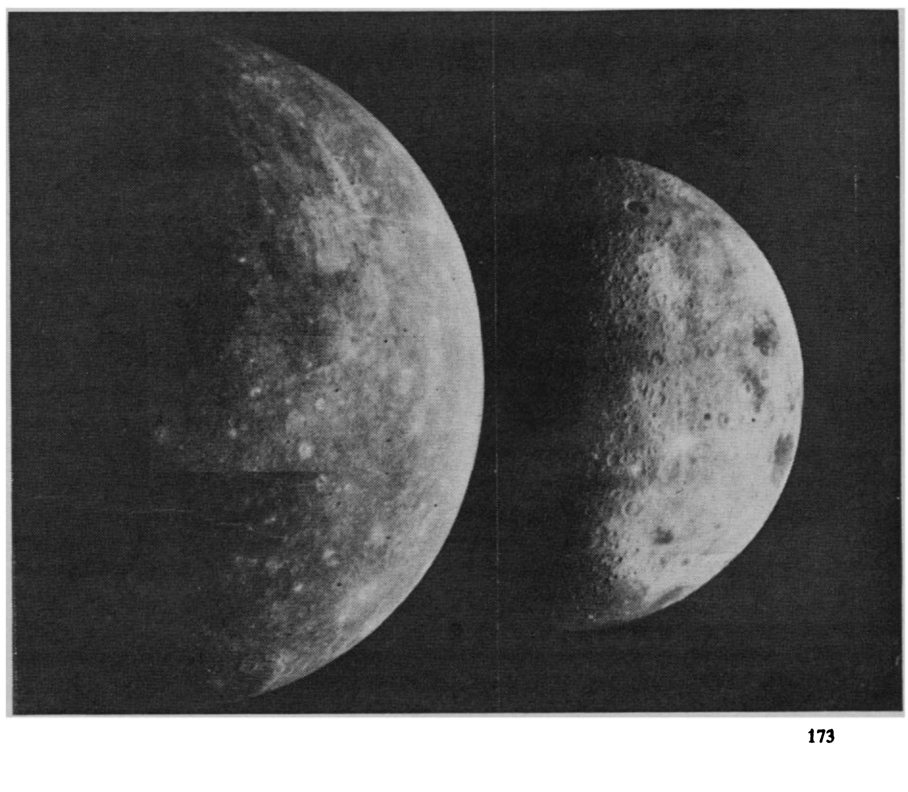

Fig. 5 (top). The incoming (right) and outgoing (left) mosaics of Mercury depicting the points of albedo measurement referred to in Table 2. The enclosed areas indicated by letters are those used in crater counting as listed in Table 3 and shown in Fig. 9. Fig. 6 (bottom). Mariner 10 pictures of Mercury (left) and the moon (right) processed to appear as they would with equal illumination. The relatively lower contrast of Mercury is apparent.

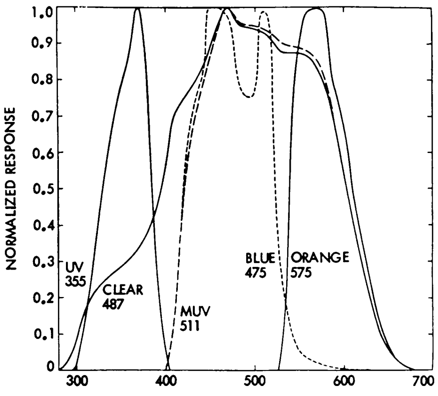

Fig. 7. The integrated optics, filter, and vidicon system response have been independently normalized for each spectral filter on the basis of the absolute Mercury spectrum and plotted as a function of wavelength. The effective wavelength (in nanometers) is shown by each filter name (*UV*, ultraviolet; *MUV*, minus ultraviolet).

Plains containing ridges and scarps surround Caloris Basin in an arcuate band from 1000 to 1500 km wide (Fig. 8 and cover). Radar studies (*12*) suggest that the band continues around at least the southwestern rim of the basin some 1000 to 2000 km on the side not illuminated at the time of the Mariner 10 flyby. In places, hills of more rugged material project through these plains, an indication that the material there is relatively thin. Caloris Basin itself is filled to within about 2 km of the highest peaks in the surrounding mountains.

The plains inside Caloris Basin contain numerous ridges and are intensely fractured (see cover). Ridges range from 1.5 to 13 km in width, have heights of about 300 m and lengths in excess of 300 km, and are grossly similar to lunar mare ridges. The extent and complexity of the ridges and associated fracturing inside Caloris Basin are greater than on lunar maria. Fractures are closely spaced with some forming a polygonal pattern; others are almost sinuous, although unlike lunar sinuous rills in detailed planimetric outline. They range in width from 6 km down to the resolution of the best photography of the basin floor (~ 700 m). The widest fractures are flat-floored and graben-like. Fractures transect, are parallel to, and even occur along the tops of ridges. The directions of fractures tend to mimic the trend of the ridges, suggesting that the structures are related. The Caloris Basin fracture pattern seems consistent with the gentle subsidence of the central part of the basin floor following emplacement of the plains. Subsidence has also affected lunar mare basins, but not to the same extent or in exactly the same pattern.

Table 4. Circular basins observed in Mariner 10 pictures (March 1974 encounter).

Feature number (Fig. 8)	Latitude	Longitude	Diameter (km)
1 (Caloris)	+30	190	1300
2	−15	165	440
3	+85	30?	350
4	−2	45	385
5	0	37	330
6	+31	159	410
7	+43	158	240
8	−18	52	220
9	−77	100	200
10	+10	190	220
11	+52	133	200
12	−64	20	250
13	−16	13	240
14	−45	178	430
15	+48	150	310
16	+27	163	240
17	+21	19	230

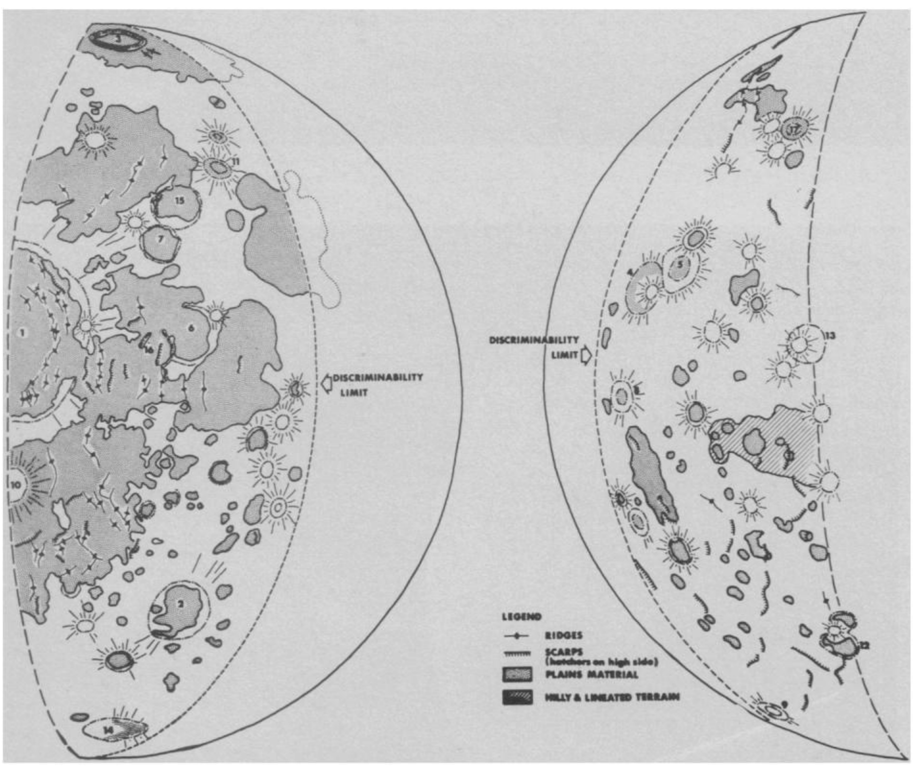

Fig. 8. Sketch map showing the major physiographic provinces on Mercury within approximately 60° of the terminator on the two hemispheres viewed by Mariner 10 and shown in Figs. 1 and 5. The rim crests of basins, arbitrarily chosen as 200 km in diameter or larger, are shown by a dash-dot symbol and keyed by number to Table 4. The more prominent craters larger than 100 km are also shown. Ejecta and secondary craters around craters and basins are indicated by radial lines.

A typical high-resolution view of two areas of plains and their surroundings (Fig. 11) shows that the rims of the enclosing craters have been battered by abundant craters not present on the younger, smooth floors. In another area (Fig. 12a) a series of filled craters shows progressively greater structural disruption of their rims, indicating a lapse of time between crater formation and filling by plains materials. These plains materials are unaffected structurally and appear to be about the same age in each depression. Later plains material fills craters and basins cut into the broad belt of earlier plains around Caloris Basin (Figs. 9 and 10).

Crater populations for plains within Caloris Basin and for surrounding plains east of Caloris (Fig. 9) are indistinguishable, an indication that the emplacement ages of the two surfaces are similar. Plains units exhibit production crater populations (*10*) in contrast to the heavily cratered terrain (Fig. 9) which is in a state of crater saturation. The mercurian plains crater populations resemble those of the more heavily cratered lunar maria. However, in any attempt to assess the absolute age of the mercurian plains through comparison of their crater number densities with those of the lunar maria, one must take into account the differences in cratering mechanics between the two bodies (*15*) as well as the possibility of differing fluxes of postaccretion impacting bodies.

Patches of plains materials on the floors of craters and basins over the rest of Mercury are indistinguishable in age or morphology from the plains concentric to and inside Caloris Basin. Some of these smaller tracts of plains materials could perhaps be impact melt from nearby craters or basins, but for many there is no well-defined source crater (Fig. 11). We have observed no direct evidence of volcanism such as cones, domes, or flow fronts. However, such lunar features are unevenly distributed and best observed under very low sun illumination. The Mariner 10 pictures of Mercury show only a single narrow band on the planet with such lighting.

The origin of the plains material is of key importance because widespread volcanism, in combination with its great bulk density, would strongly imply that Mercury is chemically differentiated. The volumes and areal distribution of the plains materials are the main arguments in favor of a volcanic origin as distinguished from an origin as solidified impact melt or debris flows. Plains materials filling Caloris Basin and the north polar basin certainly cannot be the direct result of the impact which formed these basins because the present volume of the plains fill is very close to the volume originally excavated during the cratering itself. Subsequent filling by fluid material is required, and this has been the case for Mare Imbrium, for example.

Caloris Basin, immediately after it formed, possibly resembled Orientale Basin on the moon which has experienced a minimum of volcanic filling.

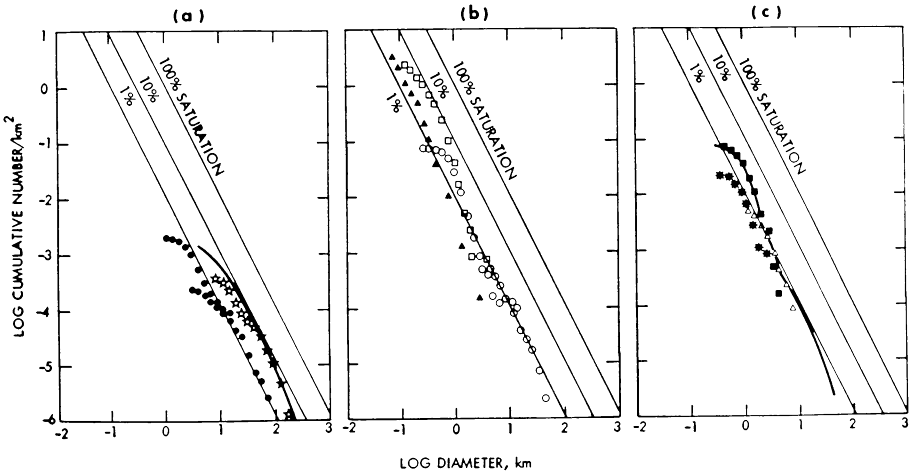

Fig. 9. Crater size-frequency distributions (for major physiographic provinces and selected areas shown in Fig. 5) are expressed as the cumulative number of craters larger than a given diameter and compared with percentages of saturation as defined by Gault (*12*). Equilibrium conditions (that is, when the rate of crater production equals the rate of crater destruction) are attained for crater populations at 5 to 10 percent saturation. Symbol notation: (a) ☆, heavily cratered terrain (area A); ●, Caloris Basin (area D); heavy line, lunar southern highlands (*24*); (b) ○, plains east of Caloris Basin (area E); ▲, Apollo 12 landing site (*23*); □, Apollo 14 landing site (*23*); (c) *, plains filling crater (area B); △, crater floor (area C); ■, plains filling crater (area F); heavy line, plains outside Caloris Basin (area E).

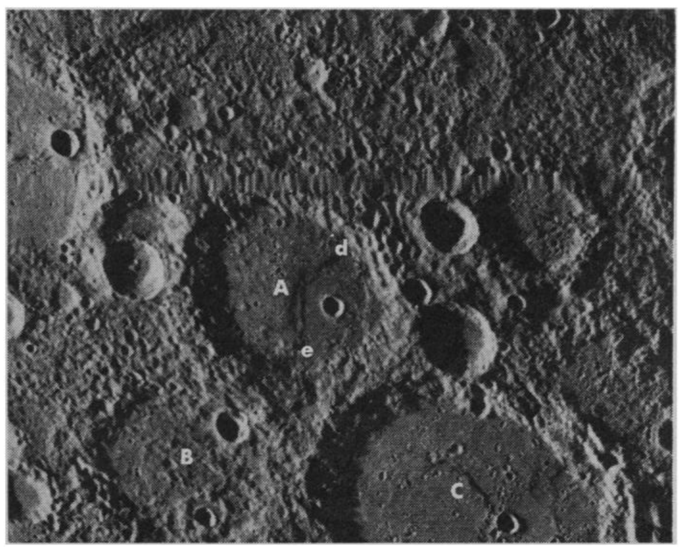

Fig. 10 (left). Typical double-ring basin 200 km in diameter (number 11, Table 4) showing a well-developed ejecta blanket (*A*) and a swarm of secondary craters (*B*). The basin is younger than the plains material to the southwest because its secondary craters overlie the plains, which, in turn, are part of a concentric band around the Caloris Basin. This double-ringed basin is also floored by plains material. North is at the top. Fig. 11 (right). Two patches of plains materials covering the floors of older craters (*A* and *C*) whose rims are much more heavily cratered. No external source for the plains material is evident. Hypothetical impact melt from crater C should have filled both craters A and B, but only crater A is filled. A volcanic origin is indicated. The scarp (*d, e*) on the floor of crater A is about 400 m high. Similar scarps have been recognized in numerous craters where they appear to be restricted to the crater floor. It is not yet clear whether they are of tectonic or volcanic origin. The blurred stripe about one-third of the distance from the top of the picture is a processing defect. Crater A is 100 km in diameter.

Orientale has numerous hummocky fissured areas on the floor and some smooth plains, probably formed from impact melt. There is also a relatively small area of dark plains (maria) believed to be of genuine volcanic origin. The volume of the Orientale melt material is insignificant compared to the volume of its impact cavity out to its outermost rim. In contradistinction, the plains concentrically surrounding Caloris Basin and the north polar basin involve enormous volumes of melted material—more analogous to the mare flooding of Oceanus Procellarum adjacent to Mare Imbrium than to the light plains materials (sometimes called Cayley Formation) containing impact breccias which concentrically surround Imbrium Basin in disconnected patches (*16*). A volcanic origin for the Caloris Basin plains and surrounding units seems to us quite probable.

Plains-filled basins conceivably may be the sites of gravity anomalies similar to the lunar mascons. O'Leary (*17*) has speculated that a nonuniform distribution of regional gravity anomalies might provide the gravitational inhomogeneity required to keep Mercury in its 3/2 spin resonant period. The location of the large Caloris Basin near the mercurian equatorial region, which is preferentially pointed toward the sun at perihelion, is suggestive in this regard. However, detailed measurements of the nonspherical portion of Mercury's gravity field (probably with an orbiting spacecraft) will be required to verify if Caloris or other circular basins on Mercury actually exhibit mascon-like gravity anomalies.

Unique surface features. Topographic forms are the signature of surface processes of construction and destruction. Features which appear unique to Mercury are therefore of special interest as they may record processes or events, or both, that have not operated on other bodies. The large scarps of great linear extent that transect both craters and intercrater areas on Mercury appear to be just such features. Several of the largest of these are indicated in Fig. 8. These scarps are best seen on the heavily cratered incoming view of Mercury. Preliminary shadow measurements indicate that several of the scarps may attain heights of 3 km or more. They generally have sinuous outlines with slightly lobate fronts and commonly attain lengths well over 500 km (Fig. 14). The scarps face in various directions, although east-facing scarps appear to be more frequent in the incoming view. Often large craters interrupt their paths, suggesting that at least some of the scarps were formed during the final stages of intense bombardment of the surface. The lobate form of the scarps, and their crater transection relation, suggests that they may be thrust or reverse faults caused by compressive stresses. If this interpretation is correct, then Mercury is the first planet other than Earth to show evidence for global compressive stresses on this scale. Such compressive deformation evidently was significant during the later phases of heavy bombardment, if not earlier.

A peculiar terrain of hills and lineations (Fig. 12, a and b), confined to a semielliptical area of at least 500,000 km^2, is centered at latitude 20°S and longitude 20°, approximately antipodal to Caloris Basin. Because the terrain extends into the terminator, the areal extent may be considerably greater. This terrain is somewhat similar to the hilly and furrowed terrain northwest of the lunar Mare Humorum (*16*). The hills are generally wider than in the lunar example; whether there are other significant differences is not clear without additional picture analysis. The hilly and lineated terrain on Mercury includes craters whose rims have been broken up into hills and depressions. Some craters are more strongly modified than others of comparable size, suggesting that this terrain developed over an appreciable period of time rather than during a single catastrophic event. The extended duration yet limited geographic distribution point toward an internal origin.

The floors of many craters in the hilly and lineated terrain are almost completely filled with plains material which embays dissected crater rims

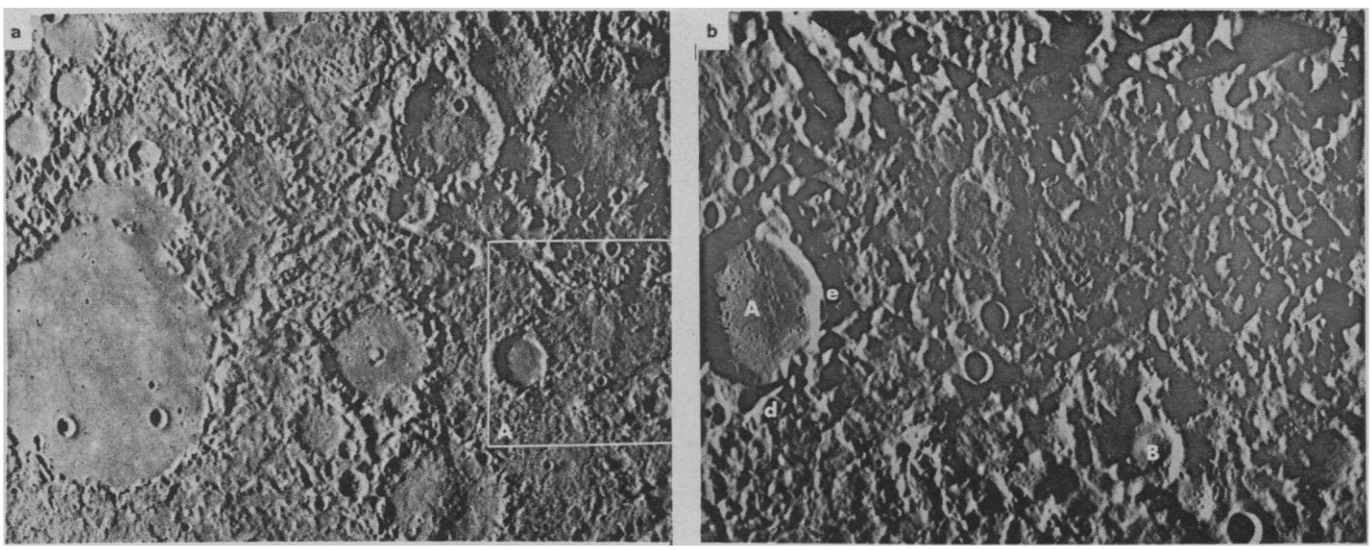

Fig. 12. (a) Hilly and lineated terrain whose distribution is shown in Fig. 8. The rims of flat-floored craters show varying degrees of structural disruption, suggesting that the terrain developed over a period of time. Plains materials on the crater floors are younger than the surrounding terrain; the plains in the largest crater (170 km in diameter) have a crater number density similar to that of the plains surrounding Caloris Basin. (b) A high-resolution (400-m) picture of area A shown in (a). This terrain consists of numerous dissected hills (~0.1 to 1.8 km high) interspersed with smooth material. The southern rim (*d*) of the 31-km crater (*A*) has been severely dissected, but the eastern rim (*e*) is largely intact. The crater rim of the smaller crater (*B*) is barely recognizable.

and is clearly younger than the hilly and lineated terrain. Hence, the formation of this terrain appears to fall between the end of heavy bombardment and the emplacement of the plains units filling the Caloris Basin and elsewhere.

Planetary history. The Mariner 10 picture data suggest to us that Mercury underwent a period of early heavy bombardment, resulting in the formation of huge basins, and that this was followed by the widespread volcanism represented by the plains materials. The inferred sequence of events is remarkably similar to that deduced for the moon; a strong chemical similarity to the moon on the scale of these plains units is also indicated. But Mercury is much denser on a planetary scale than the moon. Therefore, Mercury must be a chemically differentiated planet; silicate outer layers probably enclose an iron-rich core.

That the materials of the uppermost centimeters to meters on Mercury probably are iron silicates at least grossly similar to those on the moon (density range, 3.0 to 3.3 g/cm^3) has been known for many years on the basis of ground-based radio, radar, optical, and infrared measurements (*18*). Now, a silicate composition for at least the outer few kilometers is indicated directly by the Mariner 10 pictures because of the strong similarity in albedo and morphology of the mercurian cratered terrains and plains to those of the lunar highlands and maria. Furthermore, the resemblance of Mercury to the moon probably persists to a greater depth. Silicate material must extend to a considerable depth in order to have supplied the large amount of volcanic material that composes much of the extensive plains deposits. Indeed, Reynolds and Summers (*19*) have estimated that an iron core of terrestrial composition for a differentiated Mercury would extend outward 75 to 80 percent of the radius of the planet; the silicate outer layers would be approximately 500 to 600 km in thickness. Alternative interpretations of Mercury's internal structure fail to plausibly account for the close similarity to the lunar surface (*20*).

What additional planetary history is evidenced by Mercury's surface? A striking feature of Mercury (and of the moon as well) is that an ancient heavily cratered terrain has been preserved in extensive regions without major modification by either internal processes such as volcanism or surface processes such as atmospheric erosion. Some of the topographic features comprising such terrain are very probably of considerable antiquity, 4 to 4.5 billion years old if lunar history is relevant. Analysis of samples returned from the moon has raised the possibility that the lunar heavy bombardment may have continued until 4 billion years ago (*21*). Yet, some volcanic rocks returned from the lunar highlands may be as old as 4.5 billion years (*22*). Further resolution of the history of the moon, as well as detailed consideration of intrinsic differences in both accretion and the flux of other solar system objects at Mercury as compared to the moon, seem required before the terminal phases of heavy bombardment of Mercury can be assigned to a time period more precise than 4 to 4.5 billion years ago.

The survival of ancient cratered terrain places limits on the time when material now composing the planet became chemically differentiated. In particular, differentiation must have been complete by the time the oldest surviving landforms were created. The complete planetary heating required for in situ differentiation of an originally homogeneous planet very likely would have significantly modified all surface topography through destructive volcanism, atmospheric effects, or even melting. Consequently, the differentiation of Mercury must have occurred before the end of heavy bombardment. Furthermore, there is no evidence of any atmospheric modification of the ancient land surfaces, making it unlikely that Mercury has possessed any tangible atmosphere since the end of heavy bombardment. The most recent impact craters on Mars, for comparison, have lost their ray systems and

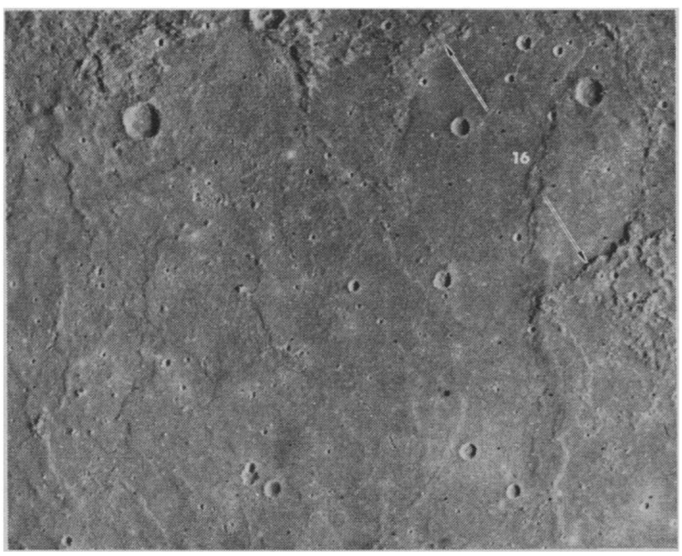

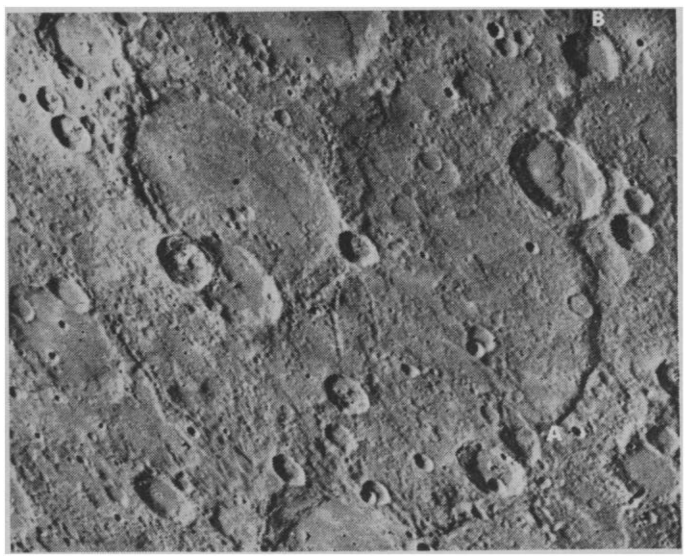

Fig. 13 (left). A 240-km basin (number 16, Table 4) almost completely floored by plains materials that are part of the concentric band around Caloris Basin. The number 16 is centered in the basin, and arrows point to a ring of low unflooded hills which define the basin. Caloris Basin lies 1300 km to the southwest. North is at the top. Fig. 14 (right). A sinuous, slightly lobate scarp (*A* through *B*) over 300 km long which transects two craters. Preliminary shadow measurements indicate a maximum height on the order of 3 km. The form, dimensions, and crater transection relations suggest that this structure (and many others of a similar nature) is a thrust or reverse fault due to compressive stresses. Craters cut by scarp are 55 and 35 km in diameter.

secondary crater chains, a result which attests to the capacity for even a very thin atmosphere to conspicuously modify cratered surfaces. To the extent that chemical differentiation can be expected to produce an atmosphere, the absence of any atmospheric erosional effects suggests that Mercury's differentiation substantially predated the end of heavy bombardment there.

The planetary-scale scarps and ridges are suggestive of a major episode of compression. The lack of recognizably similar features on either the moon or Mars suggest that these features may record an episode peculiar to the internal constitution and evolution of Mercury. An obvious speculation is that an iron-rich core underwent shrinkage, resulting in compression of the outer layers, especially if the core were as large as suggested by Reynolds and Summers (*19*). Such an episode of surface compression apparently prevailed during the terminal phase of heavy bombardment but not throughout much of the rest of the history of the planet.

The hilly and lineated terrain may reflect localized internal processes. Although we do not offer any particular suggestion on the nature of these processes, it may be significant that they also appear to have occurred during the terminal phases of heavy bombardment and not after emplacement of the plains units.

As on the moon, volcanic filling of the large basins, and emplacement of all the plains, took place after the end of heavy bombardment. Little subsequent internal or external activity is recorded in the observed portions of the planet. The sequence of events recorded on the surface of Mercury is remarkably similar to the lunar surface record. If the relationship between incident impact flux and time also proves to be similar, then the absolute time scales are comparable as well.

Of course, we have viewed only approximately 25 percent of the planet under useful viewing geometry and lighting conditions. Earlier exploration of the moon and Mars provides ample reasons for caution in generalizing planetary history from only a limited surface sample. We cannot exclude the possibility that other kinds of volcanic processes or more recent internal activity, or both, are manifested on the presently unexplored parts of Mercury. Nevertheless, the constraints on chemical differentiation and atmospheric history, and the general similarity to lunar history, remain quite valid conclusions even from the present limited surface sample since they refer to global processes.

What do these results about Mercury imply concerning the other terrestrial planets? The existence of large basins now has been recognized on the moon, Mars, and Mercury; those three bodies also exhibit striking asymmetries in their major physiographic provinces. Although not well understood, these characteristics must be acknowledged to be a rather common aspect of terrestrial planet formation. In addition, early rather than late chemical differentiation seems supported by the Mercury results. All of these circumstances may also pertain to the formation of Earth where direct information regarding these episodes is no longer available.

We have viewed a new world. Mariner 10's long reach across space has magnified our view of Mercury's surface 5000-fold and transported us back in time to the very formation of the terrestrial planets. Further study of the Mariner 10 data—and further exploration of Mercury—can sharpen and expand that view of the past, our past.

BRUCE C. MURRAY
California Institute of Technology, Pasadena 91109

MICHAEL J. S. BELTON
Kitt Peak National Observatory, Tucson, Arizona 85726

G. EDWARD DANIELSON
Jet Propulsion Laboratory, Pasadena, California 91103

MERTON E. DAVIES
Rand Corporation, Santa Monica, California 90401

DONALD E. GAULT
Ames Research Center, Moffet Field, California 94035

BRUCE HAPKE
University of Pittsburgh, Pittsburgh, Pennsylvania 15260

BRIAN O'LEARY
Hampshire College, Amherst, Massachusetts 01002

ROBERT G. STROM
University of Arizona, Tucson 85726

VERNER SUOMI
University of Wisconsin, Madison 53706

NEWELL TRASK
U.S. Geological Survey, Reston, Virginia 22092

References and Notes

1. B. C. Murray, M. J. S. Belton, G. E. Danielson, M. E. Davies, G. P. Kuiper, B. O'Leary, V. E. Suomi, N. J. Trask, *Icarus* **15**, 153 (1971).
2. B. C. Murray, M. J. S. Belton, G. E. Danielson, M. E. Davies, D. Gault, B. Hapke, B. O'Leary, R. G. Strom, V. E. Suomi, N. Trask, *Science* **183**, 1307 (1974).
3. M. E. Davis, *Icarus* **17**, 116 (1972); *Photogramm. Eng.* **39**, 1297 (1973); ——— and D. W. G. Arthur, *J. Geophys. Res.* **78**, 4355 (1973).
4. The International Astronomical Union (IAU) in 1970 defined the origin of planetographic longitudes as the meridian containing the subsolar point at the first perihelion passage of 1950 (Julian date 2433292.63) and recommended the use of a rotational period of 58.6462 days. This definition is adequate for astronomical use; however, it does not tie the meridians directly to surface features since intermediate steps of spacecraft trajectory and camera pointing angles must be known precisely. Thus, it was necessary to redefine the system of longitudes relative to a small, conspicuous crater (Hun Kal) so that the coordinate system is rigidly fixed to the surface features; a similar crater definition of longitudes was adopted for Mars in 1972 after the Mariner 9 mission [G. de Vaucouleurs, M. E. Davies, S. T. Sturms, *J. Geophys. Res.* **78**, 4395 (1973)]. This Mariner 10 Mercury coordinate system can be related to the IAU system through the control net computations, which currently give a value of 359.92 for the longitude of the prime meridian of the IAU system.
5. A. Dollfus and M. Aueriere, *Icarus*, in press.
6. G. de Vaucouleurs, *ibid.* **3**, 187 (1964); K. Hameen-Anttila and T. Pikkarainen, *Moon* **1**, 440 (1970); D. Harris, in *Planets and Satellites*, G. Kuiper and B. Middlehurst, Eds. (Univ. of Chicago Press, Chicago, 1961), p. 272; W. M. Irvine, T. Simon, D. H. Menzel, C. Pikoss, A. P. Young, *Astron. J.* **73**, 807 (1968); B. Lyot, *Ann. Observ. Paris* **8** (No. 1), 169 (1929); T. B. McCord and J. B. Adams, *Science* **178**, 745 (1972).
7. H. Pohn and R. Wildey, *U.S. Geol. Surv. Prof. Pap. 599-E* (1970).
8. The normal albedo is defined as the ratio, at zero phase angle, of the brightness of an area to the brightness of a Lambert surface viewed from the normal. The minimum phase angle at which Mariner 10 "observed" Mercury was about 75°. We estimated the normal albedo of features on Mercury by interpolation, using the lunar photometric phase function. The lunar observations made by Mariner 10 shortly after launch were used to confirm the prelaunch calibration. Normal albedos of several lunar regions were measured and compared with the Pohn-Wildey lunar albedo map (*7*) and with the measurements of Dollfus *et al.* [A. Dollfus, J. E. Geake, C. Titulaer, in *Proceedings of the Second Lunar Science Conference*, A. A. Levinson, Ed. (MIT Press, Cambridge, Mass., 1971), vol. 3, p. 2285], Bowell *et al.* [E. Bowell, A. Dollfus, J. E. Geake, in *Proceedings of the Third Lunar Science Conference*, E. A. King, Jr., Ed. (MIT Press, Cambridge, Mass., 1972), vol. 3, p. 3103], and Dollfus and Aueiere (*5*).
9. R. Greeley and D. E. Gault, *Moon* **2**, 10 (1970).
10. D. E. Gault, *Radio Sci.* **5**, 273 (1970).
11. E. M. Shoemaker, M. H. Hait, G. A. Swann, D. L. Schleicker, G. G. Schober, R. L. Sutton, D. H. Dahlem, E. N. Goddard, A. C. Waters, in *Proceedings of the Apollo 11 Lunar Science Conference*, A. A. Levinson, Ed. (Pergamon, New York, 1970), vol. 3, p. 2399.
12. R. Goldstein and S. Zohar, *Astrophys. J.* **79**, 85 (1974).
13. D. E. Stuart-Alexander and K. A. Howard, *Icarus* **12**, 440 (1970).
14. K. A. Howard, D. E. Wilhelms, D. H. Scott, *Rev. Geophys. Space Phys.*, in press.
15. The crater distribution for these mercurian plains (Fig. 9) is almost the same as that obtained for the Apollo 14 landing site (*23*); the population of mercurian craters 1 km in diameter is greater by a factor of 10 than that of the Apollo 12 site which yielded rocks with the youngest crystallization ages from the moon. Mercury's gravitational acceleration is greater than that of the moon by a factor of 2.2. This difference will tend to inhibit crater size. On the other hand, impact velocities at the sur-

face of Mercury should be greater than for the lunar case if the impacting bodies are from the same source; thus Mercury should have larger craters for impacting objects of the same mass. Although these two factors are compensating, the effects of velocity probably dominate. Mercurian craters produced by a given impacting mass plausibly could be two to three times larger than their lunar counterparts. This difference would be manifested as an increased number of craters of any given size for the same accumulated fluxes at both bodies. Thus the similarity between the frequency distributions for the Caloris plains units and Apollo 14 site is only apparent, and the implied ages would be different even if the impact flux histories could be assumed to have been the same.
16. D. E. Wilhelms and J. F. McCauley, *U.S. Geol. Surv. Map I-703* (1971).
17. B. O'Leary, *Nature (Lond.)* **220**, 1309 (1968).
18. G. P. Kuiper, *Commun. Lunar Planet. Lab. Univ. Ariz.* **143**, 165 (1970).
19. R. T. Reynolds and A. L. Summers, *J. Geophys. Res.* **74**, 2494 (1969).
20. However, at least three less likely alternative configurations of Mercury warrant brief mention. (i) Mercury has only a very thin skin of silicate material (a few tens of kilometers) residing on a substratum of undifferentiated rock (density, ~ 5.5 g/cm³); the silicates that formed the plains have been drained laterally from over a large area. (ii) The volcanic material of the plains has differentiated in situ into a lunar-like silicate phase and a much denser iron phase; the residual iron must then have moved downward tens if not hundreds of kilometers over a significant portion of the mercurian surface to permit adequate silicate melt to collect near the surface. (iii) The silicate melt that formed the plains was "sweated" out of a uniform, undifferentiated planetary mix maintained at the eutectic temperature throughout most of its mass; it is postulated that the iron component remained solid. In addition to internal difficulties each of these ad hoc possibilities seems poorly suited to reproduce in such detail both the small-scale morphology and the broad three-dimensional form of the lunar maria. The production of extensive volcanic plains requires that the temperature and composition of source materials remain relatively uniform and also requires abundant (if intermittent) flow. Whereas alternative (i) (thin skin) might provide uniform material, it seems implausible that the flow rates for entirely horizontal transport should match closely those of the lunar maria where transport has been in part, at least, vertical. Furthermore, widespread evidence of withdrawal should be present for large areas surrounding the plains units on Mercury. In fact, no such evidence is found. In situ differentiation, alternative (ii), hardly seems likely to produce a uniform melt over such large areas and extended times. A similar objection applies to alternative (iii) (sweat). In addition, vertical transport over thousands of kilometers is implied in that case, making a mare-like flow rate of melt implausible.
21. R. Tera, D. Papanastassiou, G. J. Wasserburg, *Earth Planet. Sci. Lett.* **22**, 1 (1974).
22. A. L. Albee, A. A. Chodos, R. F. Dymek, A. J. Gancarz, D. S. Goldman, D. A. Papanastassiou, G. J. Wasserburg, in *Lunar Science V, Abstracts to the Fifth Lunar Science Conference* (Lunar Science Institute, Houston, 1974), pp. 3–5.
23. D. E. Gault and R. Greeley, in preparation.
24. W. K. Hartmann, *Commun. Lunar Planet. Lab. Univ. Ariz.* **4**, 121 (1966).
25. We gratefully acknowledge the support and encouragement of the National Aeronautics and Space Administration, and specifically the untiring support of W. Cunningham and S. Dwornik, the Program Manager and Program Scientist, respectively. We extend sincere appreciation and thanks to the many individuals at the Jet Propulsion Laboratory (JPL) and the Boeing Company, who contributed to the success of Mariner 10. Valuable contributions to this report were made by our television team associates, Dr. A. Dollfus of l'Observatoire de Paris, J. L. Anderson of California Institute of Technology, R. Toombs of JPL, and Dr. J. Guest of the University of London Observatory. J. Soha, JPL, expertly chose optimum parameters for image processing; W. Sowers, U.S. Geological Survey, Flagstaff, Arizona, constructed essential mosaics of the many images; M. Malin and D. Dzurisin, California Institute of Technology, and K. Klaasen of JPL provided important data and suggestions; G. Aoyagi, Ames Research Center, counted craters with precision and patience. The manuscript benefited from suggestions and criticism by Dr. J. Dunne, JPL, Prof. G. J. Wasserburg, California Institute of Technology, Prof. G. Wetherill, University of California, Los Angeles, and Dr. J. F. McCauley, U.S. Geological Survey, Flagstaff, Arizona. The Kitt Peak National Observatory is operated by the Association of Universities for Research in Astronomy, Inc., under contract with the National Science Foundation. Contribution number 2499 of the Division of Geological and Planetary Sciences, California Institute of Technology.

5 June 1974

Mercury: Results on Mass, Radius, Ionosphere, and Atmosphere from Mariner 10 Dual-Frequency Radio Signals

Abstract. *Analysis of the radio-tracking data from Mariner 10 yields 6,023,600 ± 600 for the ratio of the mass of the sun to that of Mercury, in very good agreement with values determined earlier from radar data alone. Occultation measurements yielded values for the radius of Mercury of 2440 ± 2 and 2438 ± 2 kilometers at laditudes of 2°N and 68°N, respectively, again in close agreement with the average equatorial radius of 2439 ± 1 kilometers determined from radar data. The mean density of 5.44 grams per cubic centimeter deduced for Mercury from Mariner 10 data thus virtually coincides with the prior determination. No evidence of either an ionosphere or an atmosphere was found, with the data yielding upper bounds on the electron density of about 1500 and 4000 electrons per cubic centimeter on the dayside and nightside, respectively, and an inferred upper bound on the surface pressure of 10^{-8} millibar.*

As Mariner 10 flew by Mercury on 29 March 1974, dual-frequency radio transmissions from the spacecraft were monitored on Earth. The instrumentation and techniques for making these measurements have already been described (*1*). Mariner 10's trajectory (*2*) allowed Mercury's mass to be estimated from these data and, because the spacecraft was occulted by the planet, also afforded investigators the opportunity to measure the radius of Mercury and to detect any possible atmosphere or ionosphere. The results of the preliminary analysis of the radio data are presented in this report.

Celestial mechanics. The determination of the mass and the second-degree terms in the spherical-harmonic expansion of the gravitational potential of Mercury is one of the major objectives of the radio-science experiments. Since the analysis of these data is in the initial stages, we present only preliminary findings.

The spacecraft passed about 700 km above Mercury's surface at encounter, along a track inclined about 21° to the equator; only 1 hour from encounter on either side, the spacecraft was 36,000 km from the surface, indicating the very short period during which the Doppler tracking data are sensitive to even the second-degree terms in the gravitational field of Mercury (*3*). Of course, these data are most sensitive to Mercury's mass, and this parameter was estimated with high accuracy as follows: Doppler data from 8 days before to 3 days after encounter were used to estimate the six orbital parameters of Mariner 10 and the mass of Mercury along with various subsets of the second-degree terms of the gravitational potential. In the analyses, the coefficients of all harmonics higher than second degree were always set equal to zero, and the best available knowledge was utilized for (i) the planetary and lunar ephemerides, (ii) the rotation of Earth, (iii) the locations of the radio-tracking stations, (iv) the acceleration of the spacecraft resulting from sunlight pressure, and (v) the effect of the propagation medium on the radio signals. The observed sensitivity of the results to changes in the parameter set as well as in the data set lead us to conclude that the ratio of the mass of the sun to the mass of Mercury is 6,023,600 ± 600 (*4*), in very good agreement with the value obtained earlier from analyses of planetary radar data (*5*).

The postfit residuals from all of the Mariner 10 solutions were remarkably small, the root-mean-square value being typically only a few millihertz (*6*).

We have not yet been able to determine reliably any of the second-degree terms in the spherical-harmonic expansion of the gravitational potential. However, our preliminary analysis in-